Erosion mechanisms during abrasive waterjet machining: Model microstructures and single particle experiments

M. Mieszala[a], P. Lozano Torrubia[b], D.A. Axinte[b], J.J. Schwiedrzik[a], Y. Guo[a], S. Mischler[c], J. Michler[a], L. Philippe[a]

[a] *Laboratory for Mechanics of Materials and Nanostructures, Empa - Swiss Federal Laboratories for Materials Science and Technology, Feuerwerkerstrasse 39, Thun CH-3602, Switzerland*
[b] *Faculty of Engineering, Department of Mechanical Materials and Manufacturing Engineering, University of Nottingham, NG7 2RD, United Kingdom*
[c] *Tribology and Interface Chemistry Group, Ecole Polytechnique Fédérale de Lausanne, Lausanne, Switzerland*

Abstract

The erosion mechanisms during abrasive waterjet (AWJ) machining have been examined for a variety of materials. However, no systematic study has considered the effect of the microstructure-property relationship on the erosion mechanisms in metals. In this work, the influence of microstructure and mechanical properties on the erosion mechanisms is investigated using AWJ controlled-depth milling and single particle impact experiments performed on nanocrystalline, microcrystalline and single crystal nickel samples. The resulting footprints and subsurface microstructure evolution were analysed using advanced characterization techniques. The erosion rate of the target metal is found to correlate positively with grain size and negatively with hardness but this correlation is nonlinear. The subsurface microstructure of the single crystal and microcrystalline are altered, while only the texture of the nanocrystalline nickel is modified. The grain refinement mechanism observed

April 26, 2017

in microcrystalline and single crystal microstructure is elucidated by electron backscatter diffraction. It proceeds by the generation of dislocations under severe plastic deformation, which transforms into subgrains before forming new grains under further strain. Therefore, severe plastic deformation induced by AWJ machining leads to surface nanocrystallization and induces substantial subsurface work-hardening, as revealed by nanoindentation tests and confirmed by single particle impacts, with the consequence that the erosion rate decreases with decreasing grain size. This work clarifies the erosion mechanisms in pure metals and highlights the dynamic nature of AWJ machining as a result of the complex interplay between microstructure, mechanical properties and material removal mechanisms, providing new insights into AWJ controlled-depth milling technique.
Keywords: abrasive waterjet milling, electroplating, microstructure, plasticity, nickel, nanoindentation

1. Introduction

The development of new material processing technologies has been mainly motivated by the introduction of high performance materials with enhanced properties, which have important advantages but pose a significant challenge for manufacturing companies because they are difficult to machine. Abrasive waterjet (AWJ) machining is a promising machining process to meet such requirements owing to its versatility, since it can be used to machine advanced materials with a wide range of properties, as demonstrated by Axinte et al. (2009). The process involves low cutting forces on the target. For that reason, van Luttervelt (1989) anticipated that AWJ machining is a suitable

option to reduce mechanical damage on the workpiece. The process is also known to induce negligible thermal damage, which is a great advantage for heat sensitive parts when compared with other non-traditional methods such as laser ablation. It is also regarded as a cost efficient method because it is a fast technique and running costs are relatively low. The process is empowered by a high pressure pump (Susuzlu et al. (2004) reported pressure up to 700 MPa) that delivers water through a very small orifice, accelerating it to produce a high velocity waterjet. Abrasive particles are then entrained into the jet, forming a mixture that is a powerful energy beam that erodes the workpiece. The jet can be moved over a workpiece to either cut through or perform controlled-depth machining, i.e. milling, depending on the energy of the jet and the velocity (i.e. jet feed speed) at which it is moved along the surface of the workpiece. The jet generates an abraded footprint that depends on several process parameters, such as the jet feed speed, the pressure of the pump (directly related to the kinetic energy of the jet), the mass flow rate and size distribution of the abrasive particles, the diameter of the nozzle and other geometrical considerations of the cutting system. These parameters are chosen beforehand depending on the surface to be machined, and it has been the objective of extensive research to find suitable methods to determine the optimum parameters and tool-path strategies. Although AWJ cutting is a well-developed technology, controlled-depth AWJ milling is more complicated because it is difficult to determine the actual relation between the operating parameters and the shape of the jet footprint, as well as the evolution of such footprint when multiple jet passes overlap to generate complex 3D surfaces, as discussed in Billingham et al. (2013). The

research in this field has been mainly focused on the development of predictive mathematical models to overcome these limitations. Such models would have the capability of relating the input parameters for the system with the effect of the process on the target surface, and therefore could be used to perform complex machining tasks without performing a substantial set of experimental tests. One of the main approaches is the development of dedicated finite element analysis (FEA) methods. Elementary models consider only the impact of a single particle, such as in Li et al. (2013). A refined FE model proposed by Takaffoli and Papini (2012) model the system as a set of many particles hitting a target at high velocity. More advanced models as presented by Anwar et al. (2013) include the effect of overlapping footprints. These approaches yield reasonably good results, but they are computationally very expensive and therefore the usability is very limited. But many other mathematical techniques have been proposed for this problem. Çaydaş and Hasçalık (2008) suggested artificial neural network modelling, while Pang et al. (2012) proposed empirical models. While these models are computationally faster than FEA models, they usually require a large number of experimental tests to calibrate the model. Furthermore, these approaches rely on the mechanical properties of the target surface to perform accurate predictions, making assumptions that could lead to inconsistent models. FE models, such as the one proposed by Anwar et al. (2013), make use of a material model to account for the behaviour of the target when it is hit by the abrasive particles. It is then assumed that the target is homogeneous, and that its mechanical properties will remain stable during the process. Similarly, the empirical model proposed by Pang et al. (2012)

attempt to establish a relationship between parameters such as the target material hardness and material elastic modulus and the experimental outcome of the process, quantified as the Material Removal Rate, assuming that the target can be considered as a homogeneous workpiece with a single, and stable, value for these parameters.

Although these models may yield reasonable results, the consistency of the underlying assumption that the outcome of the machining process depends on the mechanical properties of the target material measured beforehand is not clear. The impingement of the abrasive particles on the surface could modify the grain structure of the sample, and therefore modify its mechanical properties. Previous works on plain WJ processes reported by Kong et al. (2010) and Huang et al. (2012) have shown that the microstructure plays a significant role in the erosion mechanisms (i.e. plastic deformation, intergranular cracks are observed, material removal). While this effect has been studied in detail for conventional machining processes, the effect of the microstructure has usually been overlooked in the case of AWJ machining. If Hlaváček et al. (2009) reported the effect of the microstructure on the surface integrity of the workpiece during AWJ cutting, they did not monitor the microstructural evolution during the erosion process and the potential consequences of AWJ milling to manufacture 3D parts for high performance application remain unanswered.

During AWJ machining, the surface of the target metal is subjected to severe plastic deformation. The repeated impacts of the particles could change the microstructure at the subsurface, which in turn may affect both the abrasive wear mechanisms and the mechanical properties. Severe plastic defor-

mation is known to induce surface nanocrystallization, a work-hardened layer as well as residual stresses. It is therefore necessary to study in more detail the microstructural response during AWJ machining and to understand the relation between initial material properties and abrasive wear mechanisms.

In the present paper, this issue is addressed by using a metal with model microstructures (*i.e.* a fixed composition but variable grain size), effectively isolating the effect of the process on the microstructure. It is therefore possible to determine the evolution of the mechanical properties during AWJ controlled-depth machining, and whether this should be taken into account for quantitative predictive models. The detailed information provided by this study is considered as a key element for refining predictive models for AWJ milling, as well as for estimating the final microstructure and therefore the in-service mechanical performances of metals.

2. Materials and methods

In order to investigate the effect of the microstructure of the target material during AWJ machining, a material with model microstructures is needed. A material with model microstructures is a material with a fixed chemical composition, but a controlled and tunable grain size. By changing the grain size, a grain boundary strengthening, also known as the Hall-Petch strengthening, is observed, which results in an inverse relationship between yield strength and grain size, as discussed in Hansen (2004). Previous work on AWJ machining, such as the work of Billingham et al. (2013), has been usually focused on changing the process parameters to understand their effect on the final surface. However, it is possible with tunable model microstructures

in metals to isolate the influence of the microstructure by testing different workpieces with the same composition but different grain sizes, hence mechanical properties, while keeping the operating parameters fixed. Moreover, the absence of alloying elements and the use of the same processing route for each workpiece guarantee the consistency of this methodology. In this work, nickel (Ni) was chosen to serve as target material with model microstructures. The Ni samples are synthesized by electrochemical deposition, since this technique allows to finely tune the microstructure by modifying the deposition parameters.

2.1. AWJ equipment

Extensive experimental tests have been performed with different operating parameters in order to investigate the grain size effect on AWJ machining. This makes it possible to understand how the different model microstructures respond to the impact of the AWJ. The footprint of a single jet pass, *i.e* a trench, is used for this investigation, since it is considered the most basic feature that can be machined with an AWJ machine. By doing this, it is intended to isolate the effect of the microstructure from other factors, such as non-linear behaviour of the material when multiple jet passes are overlapped as discussed by Billingham et al. (2013). An example of such feature is given in Fig. 1.

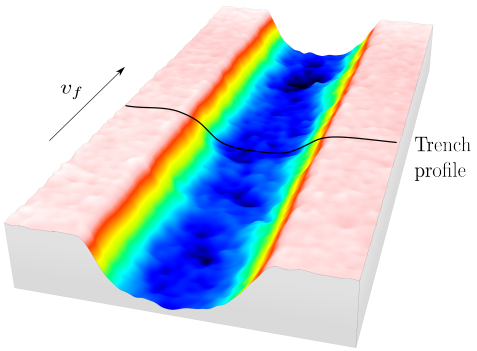

Figure 1: Example of an abrasive waterjet milled trench in Ni model material (nanocrystalline microstructure) performed at v_f = 2000 mm/min, $\dot{m}_a$ = 30 g/min and P = 1380 bar.

The experimental data for these investigations has been generated with a Microwaterjet 3-axis machine developed by Waterjet AG (shown in Fig. 2), which is powered by an ultra-high pressure pump that can deliver a pressure from 70 to 400 MPa. A jet diameter of 0.5 mm has been chosen for this work because its reduced size and good stability when used at low pressure (below 150 MPa). The abrasives used for this work are BARTON HPX #220. The pressure has been set to 138 MPa, the abrasive mass flow rate ($\dot{m}_a$) to 30 g/min, and the jet feed speeds at different values between 16.67 and 58.33 mm/s.

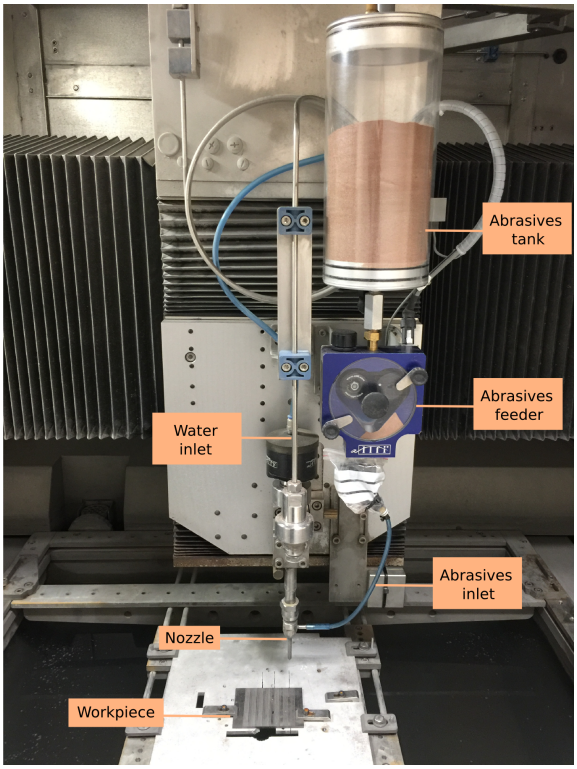

Figure 2: Abrasive Microwaterjet machine used for model validation.

2.2. Production of model materials

Microcrystalline nickel (mc-Ni) and nanocrystalline nickel (nc-Ni) samples were produced by electrodeposition in a two-electrode cell setup in which the cathode and the anode are the metal substrate and Ni-pellets contained in Ti-coated basket, respectively. The electrolyte composition includes 450 g/L of nickel sulphamate, 30 g/L nickel chloride, 20 g/L boric acid and 0.1 g/L sodium dodecyl sulphate (SDS). In order to obtain microstructure in the nanometre range, 2.5 g/L of saccharine was added to the previous bath. The temperature was kept constant at 60°C and the pH adjusted to 3.5 with sulphamic acid. Electroplating was carried out galvanostatically on a poten-

tiostat (PGSTAT30, Autolab) at -80 mA/cm^2 for nc-Ni specimens and at -500 mA/cm^2 for mc-Ni specimens. In order to complete the range of grain sizes available, a nickel single crystal (99.999 % purity) with a (111) crystallographic orientation was sourced commercially. The (111) crystallographic orientation was used because it corresponds to the texture of the electrodeposited samples. Thus the effect of texture and mechanical anisotropy on the erosion mechanism is minimized.

2.3. Specimen characterization

The samples have been analysed in detail using several techniques in order to acquire a detailed understanding of the behaviour of each model material. The surface was measured with a high-resolution chromatic confocal sensor. These measurements provide a three-dimensional map of the surface, such as the one shown in Fig. 1, and they can be used to assess quantitatively the effect of the microstucture on the erosion capability of the AWJ. Since the equipment is mounted in the AWJ machine, it can be used to measure the milled trenches in situ without manually manipulating the workpiece. A high-resolution Hitachi S-4800 scanning electron microscope (SEM) was used to examine the surface. A preliminary exploration of the surface using SEM provides a qualitative comparison of the surface of the trench, making it possible to identify the relevant differences between the samples. The microstructural evolution of the nickel samples was investigated by using ion contrast channelling images and electron backscatter images (EBSD), which can reveal information of the microstructure below the surface of the trench. Ion contrast channelling images have been obtained with a dual beam SEM-FIB Tescan Vela instrument. This is carried out by performing cross-sections

on the samples to expose the material below the surface. The cross-sections were prepared in a two-step approach. A fast cutting step with high Ga-ion beam (30kV beam and 3nA probe current) was first used to mill a rectangular trench, followed by a fine milling step (30 kV and 1nA) of the area of interest. The EBSD diffraction maps of the single crystal and microcrystalline sample were taken with an EDAX EBSD system. The EBSD maps were acquired on polished cross-sections revealing both the pristine microstructure and the microstructure modified by the action of the AWJ below the surface of the trench.

2.4. Mechanical testing

The mechanical properties of the nickel specimens were assessed before and after AWJ milling. The tests were performed with a MTS microindenter system equipped with a Berkovich indenter tip. Constant indentation strain rate of $\dot{\mathrm{P}}/\mathrm{P}{=}10^{-1}s^{-1}$ was applied by keeping the rate of load change over the instantaneous load constant up to a maximum load of 250 mN. The hardness, H, and the elastic modulus, E, were measured for each of the model materials under consideration before AWJ milling. A minimum of three indents per sample was performed and averaged. The change of microstructure induced by AWJ milling was investigated by measuring the variation of the hardness below the trench surface. Thus, the samples were cut and the cross-sections polished. An array of indents, located on the centreline of trench profile, was made on the polished cross-section. The spacing between each indent was set to 25 μm. For each indent, the method proposed by Oliver and Pharr (1992) is applied to determine the mechanical properties (hardness and elastic modulus).

2.5. Impact testing

During AWJ machining, the surface of the target material is subjected to multiple impacts at high velocity, as shown in Fig. 3a and b. Balz et al. (2013) indicated that the frequency of the impacts at any location is given by the Gaussian distribution of the abrasive particles within the waterjet. Lozano Torrubia et al. (2015) showed that the number of impacts per unit of surface can range from a few hundred to several thousand impacts depending on the processing parameters, while the particle velocity vary from 300 to 700 m/s. Each of these impacts produces a characteristic imprint in the material (Fig. 3c), whose depth depends on the mass, shape, orientation and velocity of the abrasive grit. Therefore, a single impact particle generates large plastic deformation in the material at very high strain rates, comprised between 10^6 and $10^8 s^{-1}$.

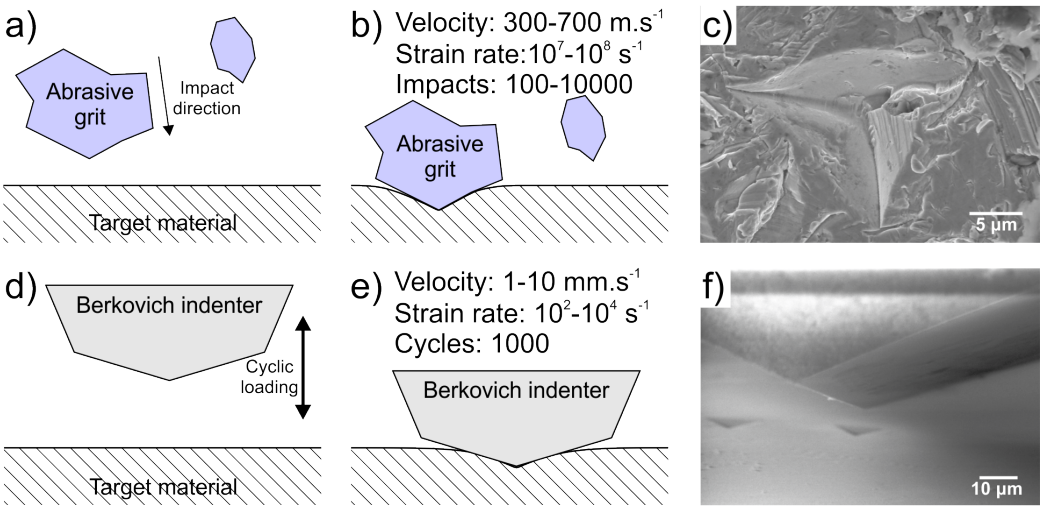

Figure 3: Schematic of (a-b) particles impacting the surface during AWJ machining and (d-e) the nanoindentation setup. SEM micrographs of a residual imprint of (c) a real single impact particle (top view) and (f) high-speed indent (cross view).

The mechanical response of metals at such strain rates differs from quasi-static experiments due to dynamic effects. Thus, if one wants to understand the mechanical response of metals during AWJ machining, high speed and high frequency instrumented indentation tests are required. However, such strain rates are not achievable with conventional nanoindentation system. For that reason, the tests were carried out on an newly developed *in situ* SEM *Alemnis* indenter using a dynamic module. The indenter was equipped with a sharp Berkovich indenter tip (three-sided pyramid), mimicking an erosive grit impacting the surface at normal angle during AWJ machining (Fig. 3d-f). Fig. 3c and f demonstrate the relevance of this approach when noting the similarities of the residual imprints of a real single impact particle and of a high speed indent. Considering that a 2 μm-depth indent is performed at an indentation speed of $1 - 10$ mm/s, the actual strain rate is $10^2 - 10^3 s^{-1}$. The indentation tests were conducted up to a maximum depth of 2μm and repeated 1000 times in 1 second for each microstructure. Subsequently, a cross-section was performed on the indents with a FIB (using a protective platinum layer), to observe the microstructure below the surface by ion channelling contrast imaging.

3. Results

3.1. Characterization of model materials

Nickel specimens with controlled microstructure, and therefore controlled mechanical properties, were generated by electrodeposition. The grain size of the sample was varied by modifying the deposition conditions and process parameters. The average grain size of the nanocrystalline specimen was

then determined by XRD analysis of the peak broadening using the Scherrer equation, finding a crystallite size of 30 nm. Quantitative X-ray measurements can then be validated by FIB observations of the microstructure. Fig. 4a shows the FIB contrast channelling image of the nanocrystalline sample, revealing homogeneous equiaxed grains. Similarly, the microstructure of the microcrystalline nickel specimen was investigated, as shown in Fig. 4b). The average grain size for this case has been estimated by image analysis of the FIB micrographs, obtaining a value of 900 nm. Apart from two model materials with different microstructure, single crystal Nickel specimens have also been used to investigate the effect of the absence of grain boundaries on the erosion process.

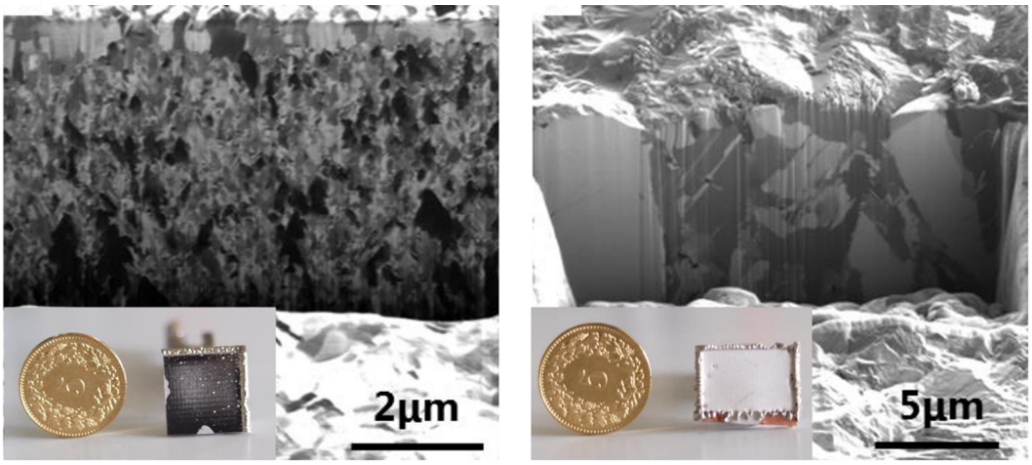

Figure 4: FIB cross-sections and ion channelling images revealing the microstructure of a (a) nanocrystalline and (b) microcrystalline nickel sample. A snapshot of the samples is included to provide with an idea of the size of the specimens.

The results from the instrumented indentation experiments are presented in Table 1 for each model material.

	Grain size (nm)	E (GPa)	H (GPa)
Single crystal Ni	NA	177 ± 2	1.20 ± 0.05
Microcrystalline Ni	900	211 ± 4	2.47 ± 0.09
Nanocrystalline Ni	30	198 ± 6	4.97 ± 0.17

Table 1: Grain size, hardness, H, and Young's modulus, E, for each nickel specimens given with the standard deviation. The nickel single crystal has a (111) crystallographic orientation.

The highest value of hardness (H=4.97 GPa) is achieved for the nanocrystalline specimen, while the one of the microcrystalline sample is only half of that (H=2.47 GPa), but twice as large as the Ni single crystal (H=1.20 GPa). The significant decrease of the hardness with the increased grain size is consistent with the grain boundary strengthening according to the Hall-Petch relationship, as discussed in Hansen (2004). The Youngs modulus of the Ni electrodeposits and single crystal Ni are also reported. The bulk isotropic value for pure nickel measured by Cantwell et al. (2012) is E=210 GPa, which agrees well with the measurements performed here. It must be noted that small deviations from the bulk isotropic value may be attributed to texture effect induced by the electrodeposition process. In the case of a single crystal material, Ledbetter and Reed (1973) demonstrated that the modulus of elasticity of face-centred cubic metal is markedly anisotropic, which explains why the Ni single crystal with a (111)-orientation has a substantially lower modulus.

The wear behaviour of metals is primarily affected by their tribological properties, and in particular the hardness. High hardness materials, such

as nanocrystalline nickel, are expected to show higher wear resistance over their polycrystalline and single crystalline nickel counterparts according to Jeong et al. (2001), resulting in a lower erosion rate during AWJ machining. However, Meyers et al. (2006) reported that the ductility of nanocrystalline metals is reduced in the nanoscale regime while Mohanty et al. (2015) showed that the strain rate sensitivity is enhanced. Therefore, the increased hardness after repetitive impacts of abrasive grits may alter the abrasive wear mechanism, from ploughing and cutting to brittle fracture. Therefore, the initial hardness of the target surface might not give a fully comprehensive view on predicting the wear resistance of the material. Even the ratio between the hardness and the modulus of elasticity, which has been suggested as a more appropriate parameter by Leyland and Matthews (2000), could be misleading since these values will evolve during the erosion process. For this reason, a broad range of characterization techniques have been used in this study, in an attempt to capture the impact of the AWJ on the material response and how this depends on the grain size.

3.2. Exploratory surface analysis

The initial phase of this investigation consisted on visual exploration of the samples using SEM. An example of AWJ milled trenches in the three model materials is given in Fig. 5. The largest difference can be observed between the single crystal nickel, Fig. 5a, and the nano-crystalline nickel, Fig. 5c. In the first case, the erosion process is thought to be mainly a plastic deformation process, since the lack of grain boundaries makes it easier for the material to deform when the abrasive particles impinge onto the surface. As the grain structure gets finer, the process is a mixture of plastic deformation

and material removal characterised by the appearance of cracks and defects in the material, yielding a smoother surface. Another significant feature is the formation of piled-up material at the edges of the trench in the single and micro-crystalline nickel samples, Figs. 5b and 5a, which indicates that plastic deformation plays a significant role in the erosion process. This has not been observed in the nano-crystalline case, Fig. 5c and this indicates that brittle erosion mechanisms predominate.

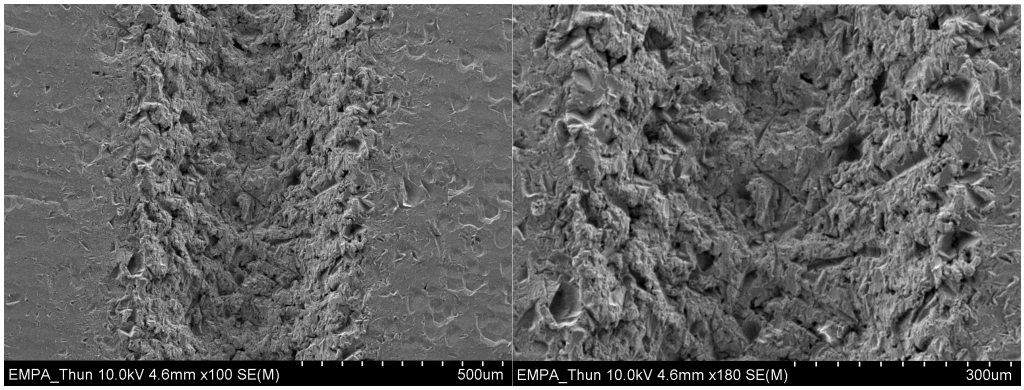

(a)

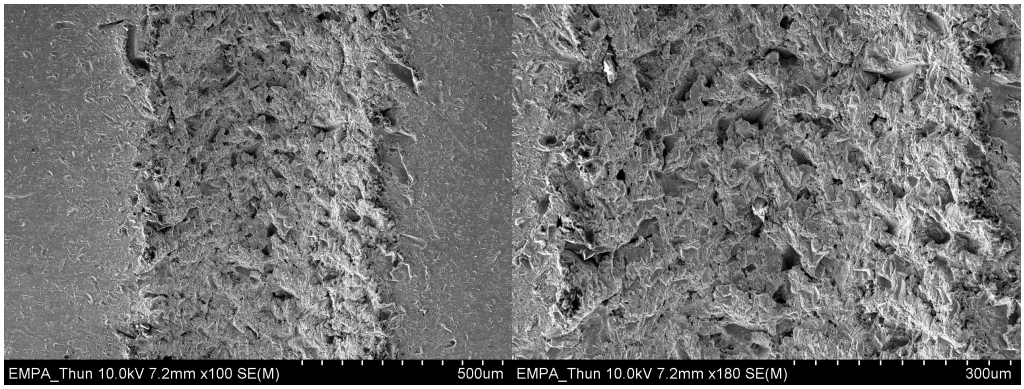

(b)

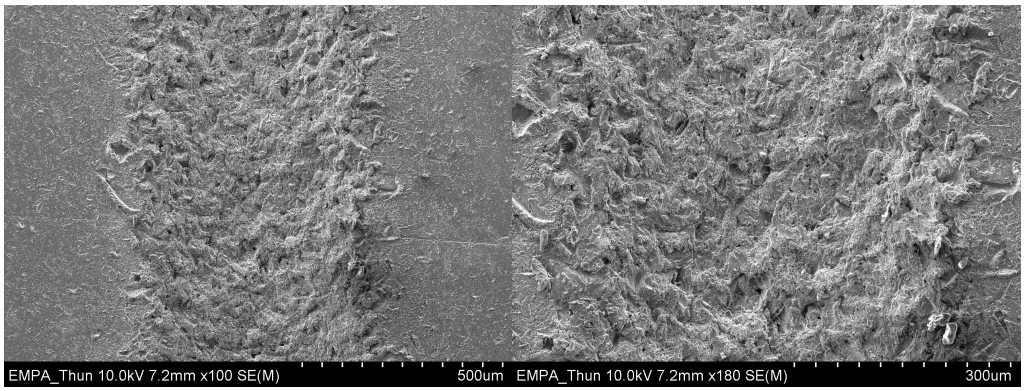

(c)

Figure 5: SEM surface observation of the waterjetted features machine at a feed speed $v_f = 2000mm/min$. a) Single crystal nickel. b) Microcrystalline nickel. c) Nanocrystalline nickel.

3.3. Quantitative analysis of abrasive waterjet milled trenches

Since all the samples have the same composition, it is considered that any difference observed between the machined features is caused by the effect of the microstructure. By looking at the material properties in Table 1, it would be expected to have a significantly larger depth in the trenches machined on microcrystalline nickel. However, it can be observed in Fig. 6 that the erosion in the microcrystalline case (Fig. 6a) is only 25 % higher than the nanocrystalline. This indicates that using such material properties to predict the erosion efficiency of the AWJ may not be a reliable method. The most remarkable difference between Fig. 6a and Fig. 6b is the shape of the average trench profiles. Firstly, it could be observed in Fig. 6a that the material piles up at the edges of the trench. This is caused by the deformation of the material generated by the load that the AWJ exerts on the sample. This feature shows evidence of ductile behaviour in the microcrystalline nickel, and it is not present in the nanocrystalline samples (6b). Secondly, the walls of the trench profile are steeper in the microcrystalline nickel. Oka et al. (1997) demonstrated experimentally that the erosion wear is more efficient as the particle impact angle increases. The erosion efficiency on the walls of the trench is therefore larger in Fig. 6a than in Fig. 6b. The morphology of the average trench profiles provides significant information of how the microstructure changes the effect of AWJ milling.

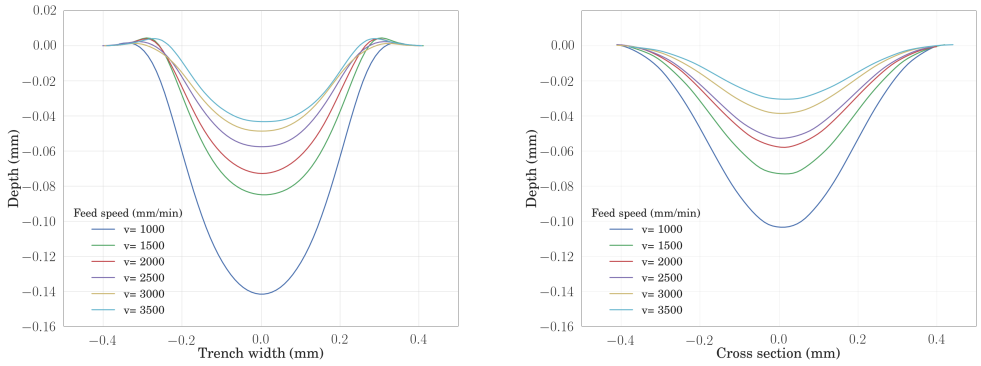

(a) (b)

Figure 6: Average trench profiles for different jet feed speeds. a) Microcrystalline nickel. b) Nanocrystalline nickel.

As mentioned earlier, both model materials have been compared to a single crystal nickel at the same feed speed, v_f= 2000 mm/min. Such comparison is shown in Fig. 7. The main conclusions that can be drawn from such comparison is that the erosion efficiency of the jet does not increase significantly from microcrystalline to single crystal nickel, although the morphology of the trench evidences that the ductile erosion modes are even more relevant, resulting in a steeper trench wall and an increase in the height of the piled up material on the edges. Although the strength of the materials is different (see Table 1), the quantitative results do not show the erosion rate to be significantly different, especially when comparing single crystal with microcrystalline nickel in Fig. 7a.

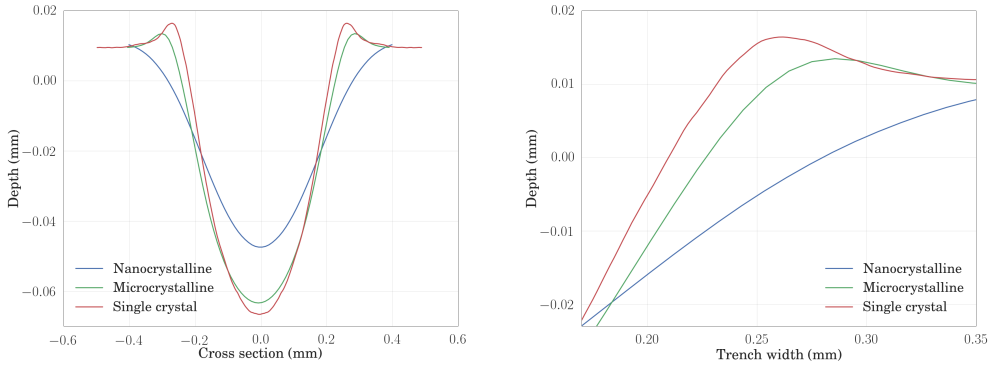

(a) (b)

Figure 7: Comparison of an average trench profile at the same jet feed speed ($v_f = 2000$ mm/min) for the three model microstructures. a) Full profile. b) Details of the edges of the trench. The ductile single crystal Ni presents large pile-up material, whereas the nc-Ni does not present this feature.

3.4. Microstructural changes leading to an understanding of the material response

A detailed characterization of the microstructure of the samples after AWJ milling was undertaken using FIB imaging and EBSD. The first step consisted on performing FIB cross sections of the AWJ milled the trenches in order to analyse the microstructure below the abraded surface. This makes it possible to use ion channelling contrast images to determine the changes of the grain size and morphology. Fig. 8 shows the microstructure below an AWJ milled trench in nanocrystalline nickel. One of the most significant features that can be observed here is the embedment of abrasive particles below the surface (see Fig. 8(2)). Moreover, the microstructure is affected by the erosion process by changing the orientation of the grains near the

surface, as it can be observed in Fig. 8(3).

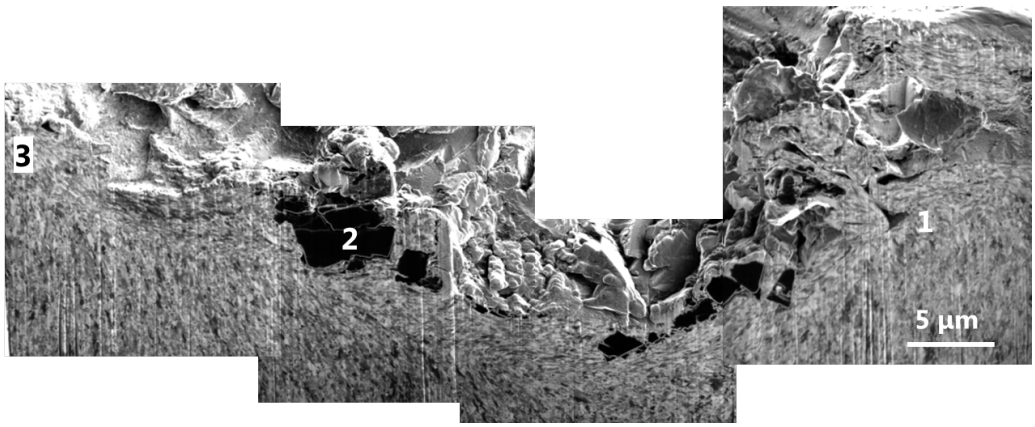

Figure 8: Ion channelling images of a nanocrystalline nickel FIB cross-sections after AWJM. Different features generated by the effect of the AWJ can be observed, such as voids (1), embedded grits (2) and grain reorientation due strong mechanical deformation (3).

Fig. 9a shows a FIB milled cross-section of a microcrystalline nickel trench. Although some of the features observed in this case are similar to the ones observed in Fig. 8, such as embedded particles, a major difference can be observed in this case: the grain structure becomes more refined near the surface of the trench, as shown in Figs. 9b and 9c. It can be noted that a fine layer of nanocrystalline grain is observed around the embedded grits (see Fig. 9c(3)), where the deformation is very high. This shows that the AWJ milling can affect strongly the material properties of the sample and provides information of how the process may occur depending on the microstructure.

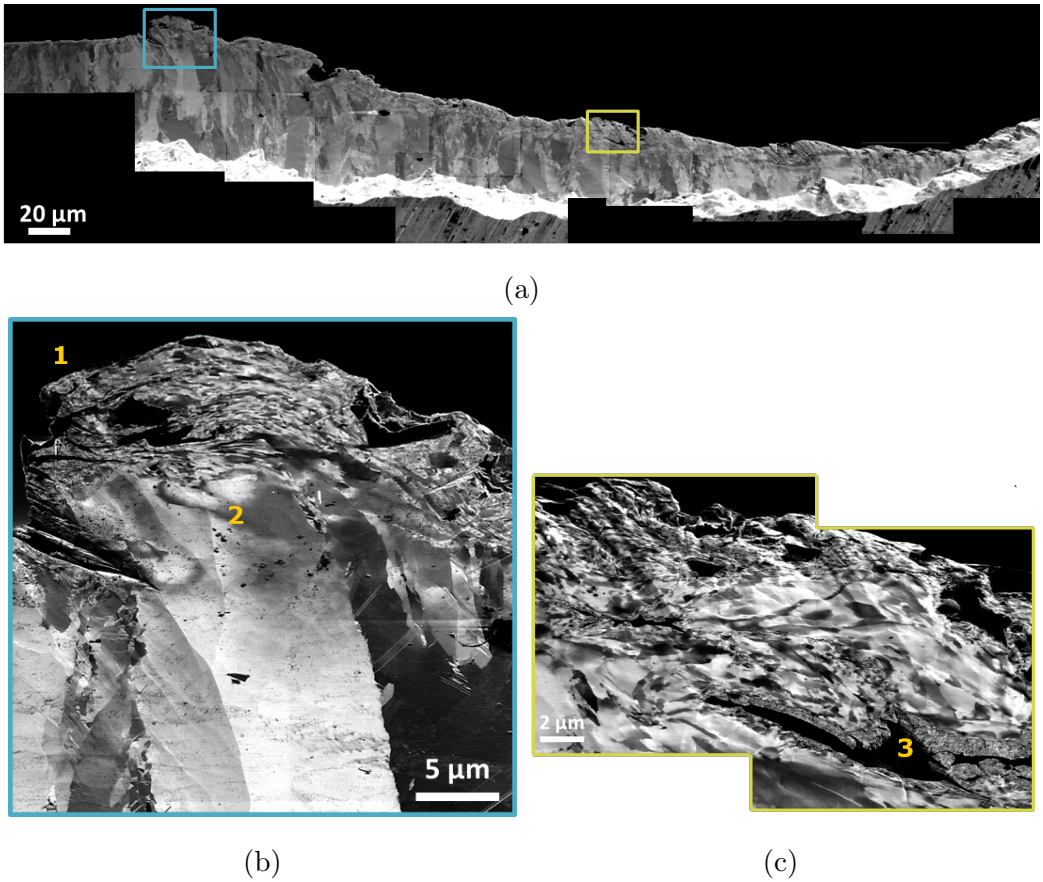

Figure 9: Ion channelling images of a microcrystalline nickel FIB cross-sections after AWJ milling. Evidence of severe mechanical deformation is observed through surface nanocrystallization. a) Cross-section showing how the large grains remain unaffected by the erosion process (2), while grain refinement can be observed near the free surface (1). b) Detail of the grain refinement near the surface. c) Detail showing the grain refining around embedded particles (3).

The analysis of the single crystal nickel offers the possibility to explain the distinct deformation mechanisms observed in the previous samples. Initially, there are no grain boundaries in the sample, but the erosion process triggers significant changes on the grain structure. Fig. 10 shows the details

of a cross section below a trench milled on a single crystal nickel specimen. It can be observed in these figures that the load of the AWJ modifies the grain structure, as well as generating imperfections and voids below the surface. The single crystal nature of the specimen is altered close to the trench surface with severe lattice distortion, extending up to 15 microns in depth. The surface alteration is characterised by various microstructural features including equiaxed nanocrystals at the surface, nanoscale deformation twins and finally accumulation of dislocation arrays.

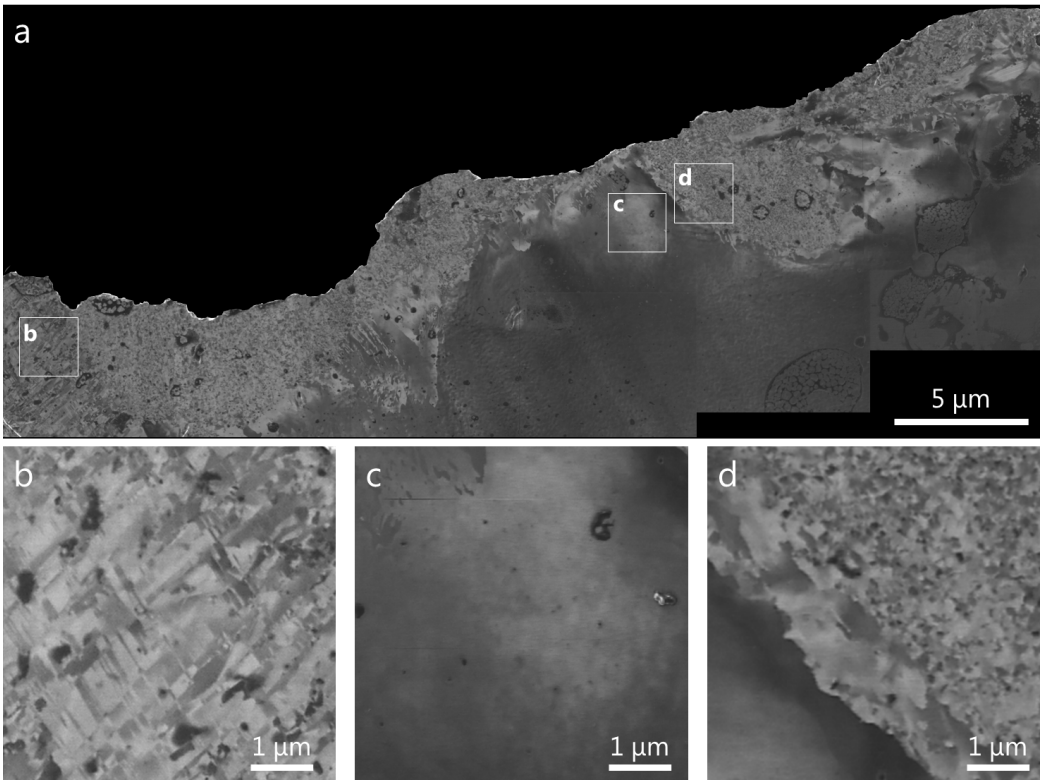

Figure 10: a) Ion channelling images of a single crystal nickel FIB cross-sections after AWJ milling. b) High-magnification image of deformation twins below the surface, resulting from the severe plastic deformations. c) The high FIB contrast below the grain-refined zone indicates high density of dislocations. d) Gradient of grain size from single crystal to nanocrystalline in the surface vicinity.

The deformation process leads to the formation of defects (i.e. dislocations and stacking faults) near the surface of the trench or at the interface between the single crystal structure and the recrystallized zone. Evidence of such dislocation accumulation is visible in Fig.10c with bright channelling contrast area. A map of the geometrically necessary dislocations (GNDs) was also derived from the EBSD measurement, as depicted in Fig. 11. An

average dislocation density of $5 \times 10^{14} m^{-2}$ was found. However, a steep gradient of dislocation density is observed near the surface. The non-uniform distribution of the dislocation density indicates that they arrange themselves in a network of dislocations, forming low-angle grain boundaries. In figure Fig.10b, deformation or mechanical twins are observed, which are characterised by lamellar structures up to a 100 nm thick and extending over several hundreds of nanometres. These represent two sets of deformation twins intersecting each other along two directions at the origin of new subgrains.

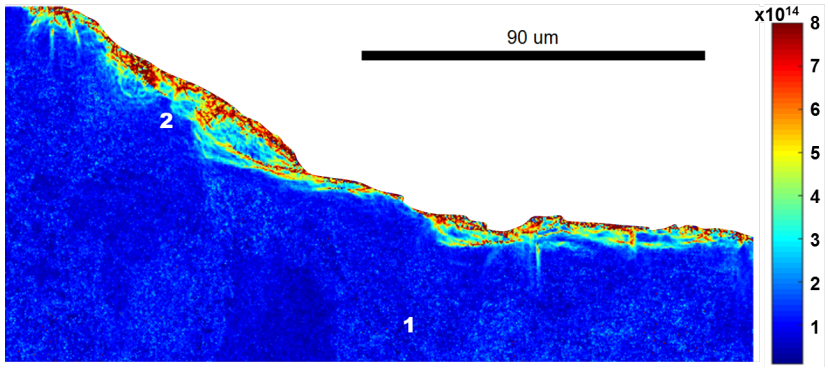

Figure 11: EBSD dislocation density map of a cross section of a trench on the single crystal nickel (expressed in dislocation/m^2). The material is mostly dislocation free (1), but the effect of the jet results in the generation of dislocations and their accumulation to form grain boundaries (2).

Yang et al. (2008) noted a grain size coarsening of electrodeposited nanocrystalline Ni induced by high strains and stresses during high pressure torsion. However, the extensive microstructural characterization of the samples revealed that the grain size in nanocrystalline samples is unaffected (even though the texture is altered) by severe plastic deformation, unlike that of the microcrystalline and single crystalline nickel. Indeed, a similar average

grain size under 100 nm was observed at the subsurface of the nc-Ni and mc-Ni samples, independently of the original microstructure. Such grain refinement and grain size saturation was reported by Hafok et al. (2006) in the case of pure face-centered cubic (fcc) metals subjected to severe plastic deformation. Pippan et al. (2010) attributed this saturation regime to the competition between dislocation nucleation and annihilation, responsible for the grain fragmentation, and recovery processes resulting in grain coarsening.

Based on the microstructural characterization of (111)-oriented single crystal, it was shown that both slip and twinning are operative to accommodate the large plastic deformation during AWJ machining. However, several parameters such as the stacking-fault energy, the strain rate and the grain size affect the twinning stress. High stacking-fault energy (SFE) materials such as nickel ($\gamma_{SFE} = 125mJ/m^2$ for Ni as calculated by Siegel (2005)) deform preferentially by glide of full dislocations rather than twinning in quasi-static conditions. However, Meyers et al. (2001) reported that the twinning stress in fcc metals decreases under dynamic loading conditions with increasing strain rates. Considering that typical strain rates are in the range of $10^5 - 10^7 s^{-1}$ for AWJ machining, twinning is expected. Based on a grain size approach, Jarmakani et al. (2008) provided a comparison of the slip to twin stress transition in nickel. When the microstructure changes from a single crystal to a nanocrystalline nickel, the twinning stress is multiplied by a factor of 5.2, consistent with FIB observations which show no evidence of twinning in the nanocrystalline sample, contrary to the other samples.

3.5. Hardness map to quantify the changes in the material properties

The mechanical properties below the surface of the trench were measured by indenting each specimen at different depths below the deepest point of the trench, as described in Sec. 2.4. A diagram to indicate the location of such measurements is embedded in Fig. 12. The values of hardness were then normalized dividing by the value of the hardness at the deepest measured point, since this makes it possible to compare the effect of the erosion process for each case. Fig. 12 shows that the normalized hardness increases dramatically for the single crystal (40%) as the depth decreases, indicating a hardening of the material. A similar pattern is observed in the microcrystalline nickel owing to the reported grain refinement. However, no hardening is observed in the nanocrystalline sample. These results confirm the observations of the microstructure, proving that the microstructure of materials with a fine grained structure will be less prone to change when impinged by an AWJ, while the generation of dislocations, new grain boundaries and the subsequent grain refinement will have an important effect on the process.

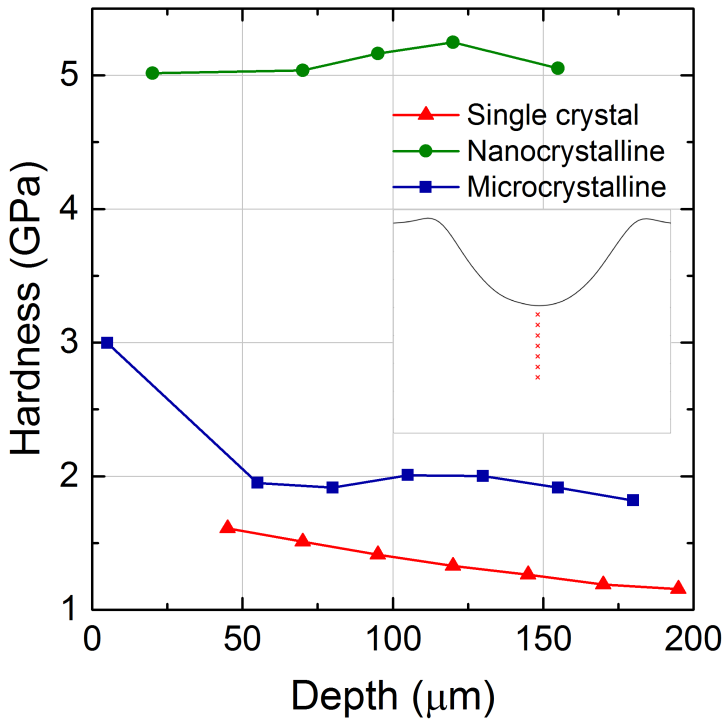

Figure 12: Indentation hardness as a function of the depth for the three different model materials. These results provide evidence of the effects of the grain refinement (mc nickel) and grain formation (single crystal nickel). The diagram is a representation of where the measurements have been taken.

3.6. Discussion of the phenomena occurring during material removal

The results obtained so far show that the microstructure of the sample does have an important effect on how the erosion process occurs. In order to understand the observations shown earlier and their relation with the grain size, a diagram of the microstructure of the model materials is given in Fig. 13a,b,c. These diagrams can be compared with the ones shown in Fig. 13d,e,f, which show the grain structure of the samples after the milling process. Firstly, the microcrystalline samples present ductile behaviour. The

effect of the AWJ deforms the material, which is pushed away creating lips of piled up material at the edges of the trench, as shown in Fig. 6a. However, the process also affects the microstructure, resulting in grain refinement near the surface, and eventually a change in the material properties of the sample, which explains why the difference in the quantitative results is not as large as it may be expected (see Fig. 13d). Secondly, the nanocrystalline nickel samples show a brittle behaviour, where material removal by attrition is the main erosion mechanism. As the AWJ attacks the surface, the material fails owing to the generation of multiple cracks, their propagation and it is eventually removed, but no grain refinement is expected (see 13e). Thirdly, the single crystal nickel sample also presents a ductile behaviour. As shown in 13c, there are not any grains in these samples initially, and the grain refinement that characterizes the microcrystalline nickel specimens is also observed here. However, as mentioned earlier, the AWJ machined samples present accumulation of dislocations, which is the preliminary step for the formation of grains. This occurs because the action of the AWJ on the material generates new dislocations, which group together in dense cell walls to form sub-grains with small misorientations, evolving eventually in high angle grain boundary, as sketched in Fig. 13f. A secondary grain refinement mechanism was identified under appropriate strain rate conditions, that is deformation twinning. The twin lamellae subdivide the microstructure into small domains, divided itself by dislocations arrays that will evolve into equiaxed grains with increasing strain.

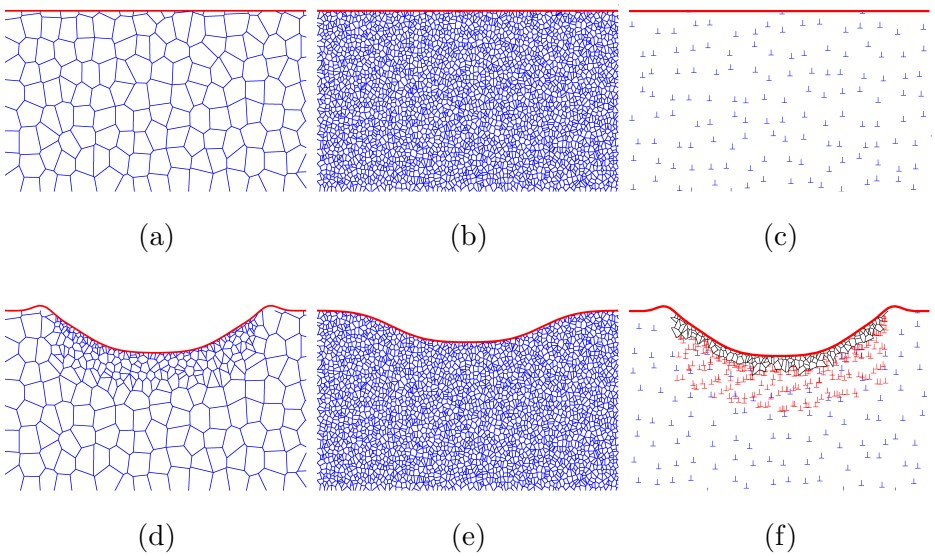

Figure 13: Schematic representation of the surface and microstucture before (a-c) and after (d-f) AWJ milling. a) Microcrystalline Ni, presenting a coarse grain structure. b) Nanocrystalline Ni, with a fine grain structure. c) Single crystal Ni, without any grains but uniform distribution of dislocations. d) Grain refinement near the surface and material piled up at the edges for mc-Ni. e) No significant change of microstructure in nc-Ni. f) Formation of dislocations (red points), leading to new grains in single crystal Ni.

The different erosion mechanisms lead to AWJ milled trenches with a significantly different morphology, as shown in Fig. 7. Fig. 7b presents a detailed comparison of the piled up material on the edges of the trench. The most ductile specimen, single crystal nickel, presents the highest piled-up material, while the behaviour of the nanocrystalline nickel is the opposite, where no material has been pushed to the edges of the trench. The grain refinement produced by the effect of the AWJ generates a gradient of mechanical properties, as shown in Fig. 12. Under the waterjet pressure the hard nanocrystalline layer transmits the energy to the underneath layer, which is

more ductile. And because of its ductility, the material is pushed away from the waterjet center line forming a material pile-up at the edge, as highlighted by Fig. 7b.

3.7. High speed indents

In order to study the effect of AWJ milling on the microstructure of the samples, it was proposed to reproduce the impact of a single particle (repeated 1000 times) using a high speed nano-indenter, as described in Sec. 2.5. Although the actual conditions of the impacts are difficult to replicate, the indents performed with this setup present a mechanical behavior and subsurface microstructure similar to the one reported in the analysis of AWJ milled samples in Sec. 3.4. Fig. 14 shows a comparison of the cross-sectional microstructure of the indents performed on the three model Ni microstructure. A change in the ion channelling contrast is observed for the single crystal nickel sample in Fig. 14a. It indicates that dislocations are generated and stored below the surface impinged by the indenter. Fig. 14b provides evidence of grain refinement near the surface of the indent for the microcrystalline microstructure, demonstrating that such mechanism could occur during AWJ milling as a result of multiple particle impacts, eventually affecting the material properties of the specimen. Similarly, the effect of the indentation on the nanocrystalline nickel, given in Fig. 14c, shows how the orientation of the grains is changed by the compressive action of the Berkovich tip.

The results obtained in this section confirm the observations in Sec. 3.4. These findings indicate that the erosion mechanisms that occurs during AWJ milling can be studied as an accumulation of multiple events (i.e. particle

impacts), that deform the workpiece, remove material and induce changes in the microstructure.

Mechanical properties measurements during the first cycle of the single impact experiment showed a significant increase in hardness for each microstructure, as compared to quasi-static measurements (see Table 1). At high strain rate, the hardness was increased by 25%, 33% and 16% for the single crystal, microcrystalline and nanocrystalline microstructure to reach 1.5 GPa, 3.3 GPa and 5.8 GPa, respectively. Under dynamic loading, Molinari and Ravichandran (2005) and Yu et al. (2013) showed that the flow stress of fcc metals is particularly sensitive to high strain rates, especially above $10^{-3}s^{-1}$ when a steep increase in flow stress is observed.

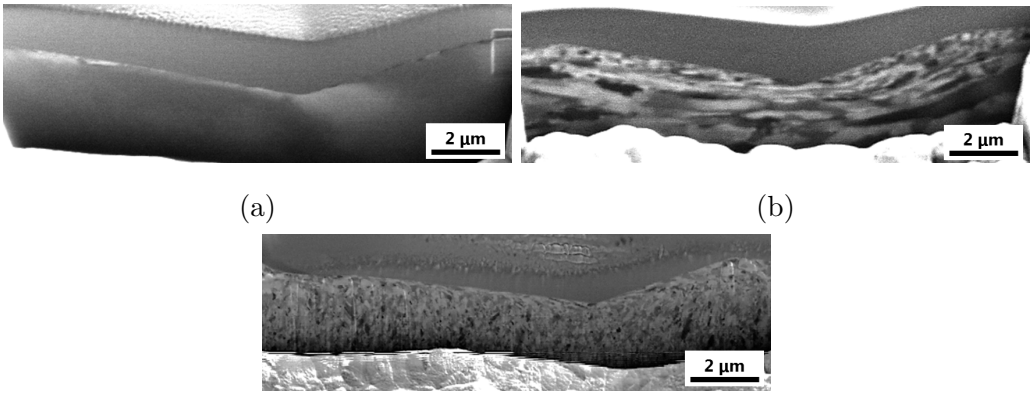

(a) (b)

(c)

Figure 14: Microstructure observation of the single impact nanoindentation. a) Single crystal nickel. b) Microcrystalline nickel. c) Nanocrystalline nickel.

This high dynamic nanoindentation technique, albeit promising, presents several limitations in its current status. First, the strain rates applied during nanoindentation (10^2-10^3s^{-1}) are lower than for AWJ machining (10^6-10^8s^{-1})

but this difference is only of 3 orders of magnitude, despite a difference of 5 orders of magnitude in velocity. Second, the geometry of the indenter tip is fixed and restricted to geometries commercially available (three- or four-sided pyramids, wedges, cones, cylinders and spheres). In reality, the abrasive grits come in all sizes and shapes, which affect the volume of eroded material according to the study conducted by Lozano Torrubia et al. (2015). In the present paper, the impinging angle is kept constant, i.e. the load is perpendicular to the sample, while the actual impinging angle is varied during AWJ machining. This limitation could be overcome by using a tilting stage. Both SEM and FIB images reveal the presence of embedded grits beneath the surface, which modify the mechanical response. Such situation cannot be mimicked by nanoindentation.

The high dynamic nanoindentation setup demonstrates the possibility to study single and multiple impact particles with defined parameters and compare them to numerical and finite elements simulations. The current experiments yield qualitative results but further development of the current setup would allow quantitative measurements of hardness at high strain rates while applying more realistic loading conditions.

4. Conclusions

In contrast to traditional methodologies that aim to study AWJ milling by investigating the effects of the operating parameters on the final surface, it is proposed in this work a novel approach that investigates the effect of the material properties, such as the hardness or the microstructure, independently from the machining conditions. This study has been performed by

generating specimens with the same composition (nickel) but different grain sizes, and then performing AWJ milling with the same operating parameters. Advanced characterization techniques have been used in order to show the effect of the grain size on the erosion mechanism and the influence of the material properties on the resulting footprints. The main conclusions of this paper can be summarized as follows:

- Specimens with a given composition may behave in a completely different manner when impinged by an AWJ if their grain size is different. This study has shown how the average trench profile in such cases may present different morphologies, and this can be difficult to predict using material properties such as the hardness. It is therefore considered that a detailed understanding of the material properties is required to develop accurate predictive models that account for the evolution of the material response during AWJ milling.

- The pressure generated by the AWJ, alongside with the effect of the abrasive grits impacting the surface, induce very high deformation inside the microstructure near the surface of the trench. To accommodate the excess strain, the material recrystallizes, resulting in a refined microstructure in this area.

- Similarly, a fine layer of nanocrystalline grain is observed around the embedded grits, where the deformation is extremely high. The fine characterization of the cross-section of the trenches shows that the material piles up at the edges of the trench because the ductile metal under the nanocrystalline layer deforms and flows towards the edges. The re-

peated impacts on the target material deform so much the surface that voids are also created.

- The characterization of the microstructure of the single crystal nickel by EBSD and FIB imaging has shed light on the grain refinement mechanisms. Firstly, the large strains induced by the impinging jet lead to the generation of dislocations. Secondly, as the strain increases, these dislocations evolve to form new grain boundaries by dislocation slip or mechanical twinning, which induces changes in the material properties of the sample.

- Although similar deformation mechanisms have already been reported for other processes, such as shot peening and equi-channel angular process (ECAP), the effect of AWJ milling on the microstructure of the workpiece has been investigated here in detail for the first time. It has been observed that the modification of the surface while milling causes strain hardening of the surface, and hence the target becomes harder and the erosion rate decreases accordingly, eventually reaching an erosion rate comparable to nanocrystalline nickel.

- The refined microstructure enhances the surface properties, while retaining the same chemical composition, with a beneficial effect on hardness, fatigue life and wear resistance. It demonstrates that AWJ machining of metals may be used in manufacturing industries to combine in a single process a milling capability with a surface treatment capability (i.e. waterjet peening).

- With the development of a high-dynamics nanoindenter, it was possible

to replicate experimentally single and multiple particle impacts at high strain rate. Subsequent microstructural observations confirmed the effect of the abrasives on the microstructure and the physical mechanisms of material removal.

From the above, it can be concluded that the contribution of this work is two-fold. Firstly, it highlights the need of performing exhaustive material characterization to understand how the process may change the material properties of the samples and how this will affect the quality of the final surface. Second, it provides new evidence on how material is eroded during AWJ in different scenarios, depending on different characteristics of the material (i.e. ductility). Future work is needed to incorporate these findings into predictive models, since taking into account the changes in the microstructure during the AWJ milling process will provide more accurate predictions and a better understanding of the process.

Acknowledgements

The authors acknowledge the financial support from the EU Initial Training Network STEEP (Grant no. 316560).

Anwar, S., Axinte, D. A., Becker, A. A., 2013. Finite element modelling of overlapping abrasive waterjet milled footprints. Wear 303 (1-2), 426–436.

Axinte, D. A., Srinivasu, D. S., Kong, M. C., Butler-Smith, P. W., Aug. 2009. Abrasive waterjet cutting of polycrystalline diamond: A preliminary investigation. International Journal of Machine Tools and Manufacture 49 (10), 797–803.

Balz, R., Mokso, R., Narayanan, C., Weiss, D. A., Heiniger, K. C., 2013. Ultra-fast X-ray particle velocimetry measurements within an abrasive water jet. Experiments in Fluids 54 (3), 1476.

Billingham, J., Miron, C. B., Axinte, D. A., Kong, M. C., 2013. Mathematical modelling of abrasive waterjet footprints for arbitrarily moving jets: Part II - Overlapped single and multiple straight paths. International Journal of Machine Tools and Manufacture 68, 30–39.

Cantwell, P. R., Kim, H., Schneider, M. M., Hsu, H. H., Peroulis, D., Stach, E. A., Strachan, A., 2012. Estimating the in-plane Young's modulus of polycrystalline films in MEMS. Journal of Microelectromechanical Systems 21 (4), 840–849.

Çaydaş, U., Hasçalık, A., Jun. 2008. A study on surface roughness in abrasive waterjet machining process using artificial neural networks and regression analysis method. Journal of Materials Processing Technology 202 (1-3), 574–582.

Hafok, M., Vorhauer, A., Keckes, J., Pippan, R., 2006. HPT-Deformation

of Copper and Nickel Single Crystals. Materials Science Forum 503-504, 621–626.

Hansen, N., 2004. Hall-Petch relation and boundary strengthening. Scripta Materialia 51 (8), 801–806.

Hlaváček, P., Valíček, J., Hloch, S., Greger, M., Foldyna, J., Ivandić, Ž., Sitek, L., Kušnerová, M., Zeleňák, M., 2009. Measurement of fine grain copper surface texture created by abrasive water jet cutting. Strojarstvo: časopis za teoriju i praksu u strojarstvu 51 (4), 273–279.

Huang, L., Folkes, J., Kinnell, P., Shipway, P. H., 2012. Mechanisms of damage initiation in a titanium alloy subjected to water droplet impact during ultra-high pressure plain waterjet erosion. Journal of Materials Processing Technology 212 (9), 1906–1915.

Jarmakani, H. N., Bringa, E. M., Erhart, P., Remington, B. A., Wang, Y. M., Vo, N. Q., Meyers, M. A., 2008. Molecular dynamics simulations of shock compression of nickel: From monocrystals to nanocrystals. Acta Materialia 56 (19), 5584–5604.

Jeong, D., Gonzales, F., Palumbo, G., Aust, K., Erb, U., 2001. The Effect of Grain Size on the Wear Properties of Electrodeposited Nanocrystalline Nickel Coatings. Scripta Materialia 44 (3), 493–499.

Kong, M. C., Axinte, D., Voice, W., 2010. Aspects of material removal mechanism in plain waterjet milling on gamma titanium aluminide. Journal of Materials Processing Technology 210 (3), 573–584.

Ledbetter, H., Reed, R., 1973. Elastic properties of metals and alloys, 1. Iron, Nickel, and Iron-Nickel Alloys. Journal of Physical and Chemical Reference Data 2 (3), 531–61.

Leyland, A., Matthews, A., 2000. On the significance of the H/E ratio in wear control: A nanocomposite coating approach to optimised tribological behaviour. Wear 246 (1-2), 1–11.

Li, W. Y., Wang, J., , H., Li, H., Huang, C., 2013. On ultrahigh velocity micro-particle impact on steels: A single impact study. Wear 305 (1 - 2), 216–227.

Lozano Torrubia, P., Axinte, D., Billingham, J., 2015. Stochastic modelling of abrasive waterjet footprints using finite element analysis. International Journal of Machine Tools and Manufacture 95, 39–51.

Meyers, M., Mishra, A., Benson, D., 2006. Mechanical properties of nanocrystalline materials. Progress in Materials Science 51 (4), 427–556.

Meyers, M. A., Vöhringer, O., Lubarda, V. A., 2001. The onset of twinning in metals: A constitutive description. Acta Materialia 49 (19), 4025–4039.

Mohanty, G., Wheeler, J. M., Raghavan, R., Wehrs, J., Hasegawa, M., Mischler, S., Philippe, L., Michler, J., 2015. Elevated temperature, strain rate jump microcompression of nanocrystalline nickel. Philosophical Magazine 95 (16-18), 1878–1895.

Molinari, A., Ravichandran, G., 2005. Constitutive modeling of high-strain-rate deformation in metals based on the evolution of an effective microstructural length. Mechanics of Materials 37 (7), 737–752.

Oka, Y. I., Ohnogi, H., Hosokawa, T., Matsumura, M., 1997. The impact angle dependence of erosion damage caused by solid particle impact. Wear 203-204, 573–579.

Oliver, W., Pharr, G., 1992. An improved technique for determining hardness and elastic modulus using load and displacement sensing indentation experiments. Journal of Materials Research 7 (6), 1564–1583.

Pang, K. L., Nguyen, T., Fan, J. M., Wang, J., 2012. Modelling of the microchannelling process on glasses using an abrasive slurry jet. International Journal of Machine Tools and Manufacture 53 (1), 118–126.

Pippan, R., Scheriau, S., Taylor, A., Hafok, M., Hohenwarter, A., Bachmaier, A., 2010. Saturation of Fragmentation During Severe Plastic Deformation. Annual Review of Materials Research 40 (1), 319–343.

Siegel, D. J., 2005. Generalized stacking fault energies, ductilities, and twinnabilities of Ni and selected Ni alloys. Applied Physics Letters 87 (12), 121901.

Susuzlu, T., Hoogstrate, A., Karpuschewski, B., 2004. Initial research on the ultra-high pressure waterjet up to 700MPa. Journal of materials processing technology 149 (1), 30–36.

Takaffoli, M., Papini, M., 2012. Numerical simulation of solid particle impacts on Al6061-T6 Part II: Materials removal mechanisms for impact of multiple angular particles. Wear 296 (1-2), 648–655.

van Luttervelt, C. A., 1989. On the Selection of Manufacturing Methods

Illustrated by an Overview of Separation Techniques for Sheet Materials. CIRP Annals - Manufacturing Technology 38 (2), 587–607.

Yang, B., Vehoff, H., Hohenwarter, A., Hafok, M., Pippan, R., 2008. Strain effects on the coarsening and softening of electrodeposited nanocrystalline Ni subjected to high pressure torsion. Scripta Materialia 58 (9), 790–793.

Yu, S.-S., Lu, Y.-B., Cai, Y., 2013. The strain-rate effect of engineering materials and its unified model. Latin American Journal of Solids and Structures 10 (4), 833–844.